Diffuse interface model for structural transitions of grain boundaries

Ming Tang and W. Craig Carter
Department of Materials Science and Engineering, Massachusetts Institute of Technology, Cambridge, Massachusetts 02139, USA

Rowland M. Cannon
Lawrence Berkeley National Laboratory, Berkeley, California 94720, USA
(Received 5 October 2005; published 4 January 2006)

The conditions for structural transitions at the core of a grain boundary separating two crystals was investigated with a diffuse interface model that incorporates disorder and crystal orientation [Kobayashi *et al.*, Physica D **140**, 141 (2000)]. The model predicts that limited structural disorder near the grain boundary core can be favorable below the melting point. This disordered material is a precursor to a liquid phase and therefore the model represents grain boundary premelting. This model is shown to be isomorphic to Cahn's critical point wetting theory [J.W. Cahn, J. Chem. Phys. **66**, 3667 (1977)] and predicts first- and higher-order structural grain boundary transitions. A graphical construction predicts the equilibrium grain boundary core disorder, the grain boundary energy density, and the relative stability of multiple grain boundary "complexions." The graphical construction permits qualitative inference of the effect of model properties, such as empirical homogeneous free energy density and assumed gradient energy coefficients, on properties. A quantitative criterion is derived which determines whether a first-order grain boundary transition will occur. In those systems where first-order transition does occur, they are limited to intermediate grain-boundary misorientations and to a limited range of temperatures below the melting point. Larger misorientations lead to continuously increasing disorder up to the melting point at which the disorder matches a liquid state. Smaller misorientation continuously disorder but are not completely disordered at the melting point. Characteristic grain boundary widths and energies are calculated as is the width's divergence behavior at the melting point. Grain boundary phase diagrams are produced. The relations between the model's predictions and atomistic simulations and with experimental observations are examined.

DOI: 10.1103/PhysRevB.73.024102 PACS number(s): 61.72.Bb, 61.72.Mm, 68.35.Rh

I. INTRODUCTION

Two-dimensional defects, such as free surfaces and internal interfaces, contribute free energy to a material system in proportion to their area. In principle, these interfaces could adopt more than one metastable "complexion" (i.e., distinct interfacial structure or composition profile). [91] Assuming that interfaces can rapidly equilibrate with their abutting phases by local atomic motion, only metastable complexions (i.e., those with local minima in free energy with respect to available degrees of freedom) will be observed. Generally, the metastable complexions, including the one with the lowest free energy (the globally stable complexion) will each have distinct, reproducibly measurable physical properties (densities, structures, compositions, etc.) that differ from those of the abutting bulk materials or crystalline phases. The complexions' stability ranking and physical properties depend on imposed constraints such as temperature, stress, and one or more chemical potentials. As in bulk-phase equilibrium coexistence, interfacial complexions could stably coexist at certain subsets of the possible values of fixed pressure, temperature, chemical potentials, etc. Grain boundary (GB) complexion coexistence identifies conditions where boundary thermodynamic properties (i.e., structure, composition, etc.) would undergo predictable alteration; derivative physical properties such as transport, creep behavior, and fracture may undergo profound changes as a consequence.

Classical (or continuum) thermodynamic considerations omit the complexity that is inherent at length scales of the order of a crystalline lattice parameter. For free surfaces of crystals, which are generally described by two geometrical variables that specify the inclination of the surface with respect to the crystal, such complexity arises from relaxation of atomic positions in the surface region. For grain boundaries, three additional parameters are required to specify the misorientation between the abutting crystals. Explicit calculations of GB structure based on atomic potentials or approximations to electron density functions provide methods for direct, often accurate, calculations of structures and excess energies, and detect short-wavelength interfacial phenomena. However—for behavior over a range of temperature, stress, chemical potentials, misorientations, and inclinations in a variety of stable crystal phases—such calculations are not feasible. Classical thermodynamics provides methods for generic stability predictions based on empirical properties. Atomistic structural and energetic calculations (which are thermodynamic minimizations in the static case) can provide information that supplements empirical data and affirm or refine continuum models.

In this paper, we extend classical interfacial thermodynamics to a simplified model of grain boundaries in fixed stoichiometric systems. The diffuse interface model is parametrized with a single misorientation variable (such as a tilt or a twist about a common crystallographic axis) and is

isotropic with respect to GB inclination. Departure from perfect crystallinity in the vicinity of a boundary is described by a spatially varying parameter that serves to characterize the "disorder" associated with a given GB structure. A resulting geometric construction predicts transitions between complexions with different disorder for a fixed misorientation and the complexion coexistence temperatures. This construction permits categorical predictions of GB transitions from qualitative aspects of empirical properties.

II. BACKGROUND

Faceting (i.e., deroughening) and premelting are examples of complexion transitions that have been observed and treated theoretically for free surfaces of pure and multicomponent systems.[3] Such transitions have also been proposed for grain boundaries.[4–6] Corroborative evidence exists but, as direct observations for GBs are much more troublesome than for free surfaces, it is often based on abrupt changes in material properties that derive from GB structure or composition.

Free-surface composition transitions are also known: for an alloy with a fixed amount of each component, the alloy's container (which may be vapor) provides an interface where stable composition gradients develop. Such transitions are treated in Cahn's critical point wetting theory (CPWT)[2] for two-component liquids, which employs a compositionally diffuse interface approximation and a molar free energy of mixing, $\Delta F(X,T)$, that gives a phase diagram with a miscibility gap.[7] For purposes of discussion, suppose the phase diagram has phase α that is rich in component A (small X) and phase β rich in B (large X) that has the lower surface energy with the container, $\gamma_{c\beta}$. For compositions within the miscibility gap, CPWT predicts a wetting transition temperature, T_{wet}, above which β is a perfect wetting phase that separates the α phase and the container (i.e., $\gamma_{c\beta}+\gamma_{\beta\alpha}\leqslant\gamma_{c\alpha}$). For the A-rich *single*-phase (α) region, a subset of compositions and temperatures, $X(T)$, exists along which two free-surface complexions, χ^{R} and χ^{P}, can coexist: χ^{R} has large B adsorption, Γ_B^{rich} and wide characteristic interfacial thickness L^{thick}; χ^{P} has smaller values of Γ_B^{poor} and L^{thin}. The curve $X(T)$ specifies locations of a first-order complexion transition between χ^{P} and χ^{R} characterized by $\Delta\Gamma_B$ and ΔL. $X(T)$ intersects the two-phase region at $(X^{\alpha},T_{\text{wet}})$. In the single-phase region between $X(T)$ and the miscibility gap, interface complexions are those χ^{R} that reflect the bulk-phase wetting behavior.[2] Such transitions have been directly observed in organic and metallic liquid systems.[8,9]

The complexion transition at $X(T)$ is an example where a *microstructural property* characteristic (e.g., absorbed layer thickness) can be superimposed onto a bulk equilibrium phase diagram. Such diagrams could be constructed whenever a microstructural defect produces local variations from equilibrium bulk compositions, structures, or other properties. Each defect (e.g., interface) feature will have characteristic quantities, such as a width and composition, that have equilibrium values and these could be included on a microstructure phase diagram. These microstructural aspects do not produce additional degrees of freedom that would modify the rules governing the topology of bulk phase diagrams. However, conditions for changes in macroscopic physical or mechanical properties that depend on microstructural features can be inferred (e.g., GB diffusivities or migration rates).

Interfacial melting is another complexion transition. Free-surface melting has been observed to initiate at temperatures T_{SM} below the bulk melting point, T_M, in various materials.[10–12] For crystals, T_{SM} can depend on interface inclination $\hat{n}$.[13,14] At $T_{SM}<T<T_M$, the stable surface configuration for a particular orientation may be a surficial film with finite equilibrium thickness, $w(T)$. The surficial film has a different structure than the equilibrium crystal phase; the structure is usually less ordered and less dense.[11,15,16] For metallic systems, as $T\rightarrow T_M$, w diverges as $w\sim w_0\ln[(T_M-T_{SM})/(T_M-T)]$ and the surficial film's structure approaches that of the liquid.[11,17–19] In addition, well below the onset of premelting, a roughening transition usually initiates for faceted or vicinal surfaces.[3,15] Finally, bulk melting usually starts from 2D defects like a free surface or GB.

Although grain boundary melting might also be expected, evidence is scant and contradictory. Observations from derivative macroscopic properties (e.g., boundary dihedral angles, GB diffusion, slidings, or migration) allude to some type of GB transitions that occur well below T_M even in nominally pure metals[20–23]—however, these could often be plausibly attributed to other causes, including kinetic transitions such as breakaway from solute clouds.[24,25] Direct TEM imaging of boundaries in aluminum specimens indicates preferential melting, but only above $0.999T_M$,[26] and, similarly, that high-angle bismuth GBs are wet by the Bi liquid at T_M.[27] Nonetheless, whether, to what extent, and in what systems GB melting actually can be observed is an open question.

These questions are addressed, but not well resolved, by numerical simulations using interatomic potentials. A lattice gas model for a tilt GB (Refs. 6 and 28) exhibits an onset of GB disorder at $T\approx 0.5T_M$, which increases towards a liquid-like state as $T\rightarrow T_M$, and the disordered region thickens as $w_0\ln[T_M/(T_M-T)]$. A number of molecular dynamics (MD) simulations using empirical potentials have also found that various high-angle GBs tend to increase continuously in disorder with rising temperature,[29–32] though some others report that GBs do retain significant crystallinity at temperatures close to T_M.[33,34] These simulations suggest that GB melting is continuous. Other simulations indicate that a first-order transition occurs rather than continuous disordering[35] and give wide boundaries well below T_M.[36] Such inconsistencies might originate from numerical artifacts, failure to ascertain the thermodynamic melting point due to finite simulation size, superheating, use of different boundary conditions, differences in atomic potentials used, and difficulties in achieving the lowest energy equilibrium structures.[34,37–39] Furthermore, a standard measure or algorithm for departure from crystallinity has not been elucidated. Nonetheless, some MD or Monte Carlo (MC) simulations detect multiple structures that are demonstrably metastable.[40–44] Additional indications for a GB structural transition are associated with discontinui-

ties in activation energies for GB diffusion or migration.[45–47]

In this paper, a diffuse interface model—based on the polycrystalline phase-field model from Kobayashi, Warren, and Carter (KWC)[1,48,49]—is used to develop a thermodynamic construction to predict GB premelting, often associated with distinct order-disorder transitions. The thermodynamic construction extends previous work of Lobkovsky and Warren that established, and numerically demonstrated, premelting near T_M.[50] Our construction becomes identical to CPWT (Ref. 2) if GB disorder is replaced with surface adsorption. Several predictions emerge herein. Boundaries tend to disorder when a disordered phase (liquid or amorphous) has a molar free energy, F^{dis}, that is not too much greater than that for the stable crystal F^{xtal}—as would pertain at temperatures and pressures near a coexistence line, or when a highly ordered GB has a large energy, γ_{GB}, related to a large dependence on misorientation $\gamma_{\mathrm{GB}}(\Delta\theta)$. This paper verifies and quantifies a heuristic argument that such transitions could occur if $\gamma_{\mathrm{GB}}(\Delta\theta)\approx 2\gamma_{sl}+w\Delta F$ (at large $\Delta\theta$) where w is an equilibrium width for the disordered region and γ_{sl} is the superficial energy density of the liquid- (or amorphous-) crystalline interface. Furthermore, stable boundaries may have *intermediate* structures between fully disordered structures and perfectly crystalline structures. A set of general GB phase diagrams is also derived.

Finally, the construction developed herein pertains to material systems with fixed stoichiometry everywhere. As more degrees of freedom appear, interface complexion transitions will become more intricate and conditions for their appearance less exceptional. For metals, and especially ceramics, empirical evidence for GB transitions is more abundant, direct, and compelling for systems wherein GBs can adjust both their structure and composition.[51–58] Generalizations and extensions to the present theory, to be published in a sequel, are consistent with such observations.

III. THEORY

In the KWC model, the free energy of a two-dimensional polycrystalline structure is a functional of two field variables, which are the local crystallinity field $\eta(\vec{x})$ and orientation field $\theta(\vec{x})$. The orientation field, θ, is a local coarse-grained measure of the "most likely" crystallographic orientation with respect to a fixed axis. [92] The crystallinity η is a coarse-grained scaled measure of structural disorder. A possible coarse-grained scheme is discussed in the Appendix. The values $\eta=1$ and 0 are usually defined as denoting crystalline and liquid states, respectively. A GB in the KWC model is a place where local crystallinity takes values between 0 and 1 and the local orientation exhibits a change from one value to another. Although fine structure characteristics of grain boundaries are eliminated by the coarse-graining procedure, features such as GB thickness and average crystallinity are retained and allow predictions of macroscopic trends.

As derived for the KWC model, the free energy functional that, at equilibrium, obtains a minimum with respect to $\theta(x)$ and $\eta(x)$ is[1,49]

$$F[\eta,\theta;T]=\int_{\mathcal{V}^{\mathrm{sys}}}\left(\Delta f(\eta,T)+\frac{\nu^2}{2}(\nabla\eta)^2+sg(\eta)|\nabla\theta|\right)dV$$
$$=A\int_{\mathcal{L}^{\mathrm{sys}}}\left[\Delta f[\eta(x),T]+\frac{\nu^2}{2}\left(\frac{d\eta}{dx}\right)^2+sg[\eta(x)]\times\left|\frac{d\theta}{dx}\right|\right]dx \quad (1)$$

where the second integral in Eq. (1) is the one-dimensional model to be employed herein. All fields are uniform in the GB plane, which is taken to be normal to the x coordinate. In the following, A is set to be unit area.

The integrand that defines $F[\eta,\theta;T]$ is a low-order approximation to the inhomogeneous free energy density, i.e., the integrand includes the values of η and θ and their spatial derivatives; the temperature T is assumed to be uniform. The differing gradient forms, $|\nabla\theta|$ and $(\nabla\eta)^2\equiv\nabla\eta\cdot\nabla\eta$, follow from KWC and are discussed briefly below as well.

The homogeneous free energy per unit volume, $f(\eta;T)$, is the free energy density of a uniform material with disorder characterized by η at temperature T. Then, Δf is defined here as $f(\eta;T)-f(\eta=1;T)$, i.e., the reference state is a single crystal (with uniform $\eta=1$ and $\theta=$const). Thus, Eq. (1) is an excess quantity describing all the interface contributions. Because F must be rotation invariant, Δf must be independent of θ: $\Delta f=\Delta f(\eta,T)$. To model boundary disordering transitions, $\Delta f(\eta,T)$ is assigned the form of a triple well with equal minima at $\eta=\pm1$ and is symmetric about another minima at $\eta=0$. (n.b. The negative η are introduced as suggested in the Appendix, but positive values of η are meaningful in this model.) At $T<T_M$, $f(\eta=1)-f(\eta=0)\equiv\Delta f^{\mathrm{devit}}<0$—the free energy density change upon devitrification is negative. We assume that point defects in the proximity of an interface obtain equilibrium concentration profiles, and these equilibrium fields are implicity included in Δf. By extending Δf to be a function of defect and solute concentrations, the effects of their spatial variation on the stability of GB structures would be an extension of the current model framework. Similar extensions that include stresses are possible. It is assumed in this paper that kinetic mechanisms allow atomic transport between the bulk and the interfaces. Therefore, interfacial stress reduces to interfacial tension. Constraints on such transport or upon the number of surface sites would require extension of this model to cases where interfacial stresses are included.

ν and s, the remaining parameters in Eq. (1), scale the gradient penalty contributions relative to the homogeneous free energy for the disorder and orientation gradient penalties, respectively. The prefactor function, $g(\eta)$, designates the effect of disorder on reducing the orientation gradient penalty: there should be no orientation gradient penalty at complete disorder and it must only increase to a maximum at $\eta=1$. A quadratic form $g(\eta)=\eta^2$ has been used for phase-field simulations,[1,49,50,59] but this will be generalized below.

To model a bicrystal with a planar lying GB normal to the x axis, the boundary conditions

$$\eta(x=\pm\infty)=1,\quad \theta(x=-\infty)=\theta_-,\quad \theta(x=\infty)=\theta_+ \quad (2)$$

are used. Assuming symmetry about the GB and that η attains its only minimum at the boundary core, only the posi-

tive axis is necessary and boundary conditions Eq. (2) become

$$\eta(x=0)=\eta_{\mathrm{GB}},\quad \eta(x=\infty)=1,\quad \theta(x=0)=\theta_+-\frac{\Delta\theta}{2},$$
$$\theta(x=\infty)=\theta_+, \tag{3}$$

where $\Delta\theta\equiv\theta_+-\theta_-$ and $\Delta\theta>0$ is assumed with no loss of generality.

Equilibrium is obtained when $F(\eta,\theta;T)$ in Eq. (1) is minimized with respect to the functions η and θ subject to Eq. (3). Because of the $g(\eta)|d\theta/dx|$ term, plus the assumptions that $g(\eta)$ is monotonically increasing and that $\eta(0)=\eta_{\mathrm{GB}}^{eq}$ is the only minimum, the equilibrium θ field localizes *all* of its change at the minimum of η,[1,60] giving

$$\theta^{eq}(x)=\begin{cases}\theta_-, & -\infty<x<0,\\ \theta_+-\dfrac{\Delta\theta}{2}, & x=0,\\ \theta_+, & 0<x<\infty.\end{cases} \tag{4}$$

The GB is isotropic as $sg(\eta)$ in Eq. (1) is independent of the boundary inclination, ψ: $\tan(\psi)=(\partial\eta/\partial x)/(\partial\eta/\partial y)$ and of the particular crystallographic orientation of either grain (θ_- and θ_+).

Combining Eqs. (4) and (1) with the relation $d\theta^{eq}/dx=\Delta\theta\delta(x)$ [i.e., $\int h(x)\delta(x-x_\circ)dx=h(x_\circ)$] produces a functional in $\eta(x)$,

$$F=s\Delta\theta g(\eta_{\mathrm{GB}})+2\int_0^\infty\left[\Delta f(\eta)+\frac{\nu^2}{2}\left(\frac{d\eta}{dx}\right)^2\right]dx, \tag{5}$$

which remains to be minimized with respect to $\eta(x)$ and the unknown η_{GB}. The first term in Eq. (5), $s\Delta\theta g(\eta_{\mathrm{GB}})$, derives from the boundary condition and favors the smallest possible η_{GB} value (i.e., $\eta_{\mathrm{GB}}=0$, a disordered GB). The integral in Eq. (5) favors a homogeneous crystal [i.e., $\eta(x)=1$]. The equilibrium GB crystallinity, η_{GB}^{eq}, results from the competition between these two terms.

The energy functional, Eq. (5), is exactly the same as that used in CPWT,[2]

$$F=\Phi(c_s)+\int_0^\infty\left[\Delta f(c)+\kappa\left(\frac{dc}{dx}\right)^2\right]dx, \tag{6}$$

if the concentration in a two-component fluid, c, is exchanged for crystallinity η. In CPWT, the short-range surface interaction $\Phi(c_s)$ term favors a composition profile with the surface adsorption, c_s, at the minimum of Φ. The integral in CPWT similarly favors a uniform bulk. This analogy suggests, under some conditions, that first-order GB structural transitions may exist at temperatures below that where the boundary is completely wet by the crystal's equilibrium melt as a parallel to the first-order adsorption transitions in CPWT.

The following graphical construction, similar to Cahn's analysis for CPWT, determines the conditions for this transition. The $\eta(x)$ that minimizes Eq. (5) has a vanishing variational derivative (c.f. Ref. 61), which requires

$$\nu^2\frac{d^2\eta}{dx^2}=\frac{\partial\Delta f}{\partial\eta}\quad\text{for } x>0, \tag{7}$$

and its variable boundary condition is subject to

$$\left.\frac{d\eta}{dx}\right|_{x=0^+}=\frac{s\Delta\theta}{2\nu^2}\left.\frac{dg}{d\eta}\right|_{\eta=\eta_{\mathrm{GB}}}. \tag{8}$$

Multiplying Eq. (7) by $d\eta/dx$ and integrating once yields

$$\frac{\nu^2}{2}\left(\frac{d\eta}{dx}\right)^2=\Delta f(\eta)\quad\text{for } x>0, \tag{9}$$

where the integration constant is determined to be zero because $\eta(x=\infty)=1$, and $\Delta f(\eta=1)=0$. As $d\eta/dx>0$ for all $x>0$, Eq. (9) is equivalent to

$$\frac{d\eta}{dx}=\sqrt{\frac{2\Delta f(\eta)}{\nu^2}}\quad\text{for } x>0, \tag{10}$$

and its integral gives an implicit solution for the equilibrium profile:

$$x(\eta)=\int_{\eta_{\mathrm{GB}}}^{\eta}\sqrt{\frac{\nu^2}{2\Delta f(\eta')}}d\eta'. \tag{11}$$

By inserting the following identity,

$$g(\eta)=\int_0^\eta\frac{dg}{d\eta'}d\eta', \tag{12}$$

and Eq. (9) into Eq. (5) and changing the integration variable from x to η,

$$\frac{F}{2}=\int_0^{\eta_{\mathrm{GB}}}\frac{s\Delta\theta}{2}\frac{dg}{d\eta}(\eta)d\eta+\int_{\eta_{\mathrm{GB}}}^1\sqrt{2\nu^2\Delta f(\eta)}d\eta, \tag{13}$$

F becomes the sum of two integrals. The only unknown quantity in Eq. (13), η_{GB}, is determined by inserting Eq. (10) into Eq. (8),

$$\sqrt{2\nu^2\Delta f(\eta_{\mathrm{GB}})}=\frac{s\Delta\theta}{2}\left.\frac{dg}{d\eta}\right|_{\eta=\eta_{\mathrm{GB}}}. \tag{14}$$

The η_{GB} that satisfy Eq. (14) are η_{GB}^{eq}.

An example of $\eta(x)$ and $\theta(x)$ solutions appears in Fig. 1.

Because $\eta_{\mathrm{GB}}=0$ bounds the range of possible values of η_{GB}^{eq}, it may itself be an equilibrium value if the extremal values of F [i.e., extremal with respect to variation of $\eta(x)$] comprise an increasing function of η_{GB}^{eq} near $\eta_{\mathrm{GB}}^{eq}=0$. For such "boundary extrema," the condition Eq. (14) will be replaced by an inequality. To find this inequality, consider two extremal solutions to Eq. (5), $\eta_0(x)$ and $\eta_+(x)$, with *fixed* boundary conditions at $x=0$: $\eta_0(x=0)=0$ and $\eta_+(x=0)=\delta\eta_{\mathrm{GB}}$, where $\delta\eta_{\mathrm{GB}}$ is a positive infinitesimal quantity. Because the variational extremum still holds, Eqs. (7) and (13) hold for $\eta_{\mathrm{GB}}=\eta_0$ and η_+. The corresponding values of F are

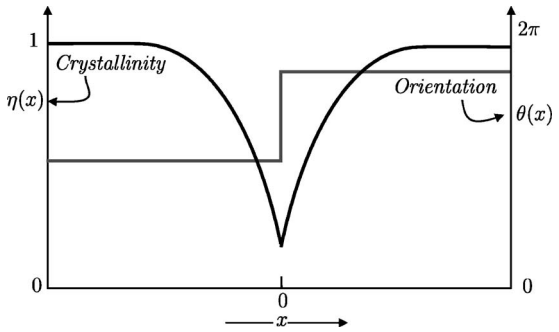

FIG. 1. Equilibrium profiles for $\eta(x)$ and $\theta(x)$ for a one-dimensional symmetrical GB. The discontinuity in first derivatives of η, which is collocated with the discontinuity of θ at the boundary core, $x=0$, is a consequence of Eq. (8).

$$F_0 = 2\int_0^1 \sqrt{2\nu^2\Delta f(\eta)}\,d\eta$$

$$F_+ = 2\left(\int_0^{\delta\eta_{\mathrm{GB}}} \frac{s\Delta\theta}{2}\frac{dg}{d\eta}d\eta + \int_{\delta\eta_{\mathrm{GB}}}^1 \sqrt{2\nu^2\Delta f(\eta)}\,d\eta\right)$$

$$= 2\left[\left(\frac{s\Delta\theta}{2}\left.\frac{dg}{d\eta}\right|_{\eta=0} - \sqrt{2\nu^2\Delta f(0)}\right)\delta\eta_{\mathrm{GB}} + \int_0^1 \sqrt{2\nu^2\Delta f(\eta)}\,d\eta\right]. \quad (15)$$

$F_+ - F_0$ is the minimum increase of excess energy for a small positive departure $\delta\eta_{\mathrm{GB}}$ away from $\eta_{\mathrm{GB}}=0$. Therefore, the condition that $\eta_{\mathrm{GB}}=0$ is a boundary minimum is

$$\frac{s\Delta\theta}{2}\left.\frac{dg}{d\eta}\right|_{\eta=0} - \sqrt{2\nu^2\Delta f(0)} > 0. \quad (16)$$

As $g(\eta)$ is a monotonically increasing function, its leading order behavior at $\eta=0$ is $g(\eta)=\eta^p$ with $p>0$. The boundary-minimum condition, Eq. (16), is never satisfied for any $p>1$ below T_M. For $p=1$, the inequality is met within a range of temperatures below T_M where $\Delta f(0)$ is small enough. For $0<p<1$, the inequality is met for all $T<T_M$. On the grounds that completely disordered boundaries are minimizers for large undercoolings if $p\leqslant 1$, this range can be eliminated because it produces unphysical results. Therefore, in the remainder of this paper, the following power law behavior for $g(\eta)$ at $\eta=0$ is used

$$g(\eta) = \eta^p, \quad p > 1. \quad (17)$$

An inequality opposite to that in Eq. (16) applies at $\eta=1$, but has no consequence in this model.

A *graphical construction*, to permit assessment of solutions, is obtained from Eqs. (13) and (14). The equilibrium value of crystallinity at the GB core, η_{GB}^{eq}, and the value of the GB energy can be represented by plotting the two integrands in Eq. (13) against the integration variable η (see Fig. 2). According to Eq. (14), η_{GB}^{eq} is determined by the intersection of the curves for $(s\Delta\theta/2)dg/d\eta$ and $\sqrt{2\nu^2\Delta f}$. According to Eq. (13), one-half the GB energy, $F/2$, is the area under

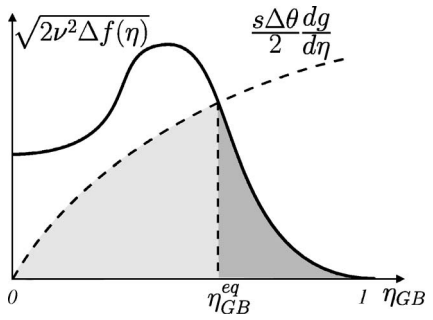

FIG. 2. Graphical construction for GB complexions [see Eqs. (13) and (14)]. The equilibrium GB crystallinity, η_{GB}^{eq}, is the intersection of the curves represented by the integrands in Eq. (13) and the sum of the two shaded areas is half of the free energy of an equilibrium GB.

the first curve between 0 to η_{GB}^{eq} plus the area under the second curve from η_{GB}^{eq} to 1. This representation demonstrates the competition between the boundary condition and the bulk integral terms in Eq. (5): The boundary condition term, arising from the region $0<\eta<\eta_{\mathrm{GB}}^{eq}$, and the bulk term, from $\eta_{\mathrm{GB}}^{eq}<\eta<1$, are directly coupled through η_{GB}^{eq}.

The graphical construction permits prediction of trends in the temperature dependence of GB complexions based on qualitative aspects of the assumed double-well form of $\Delta f(\eta)$ and of the monotonic, temperature-insensitive, behavior of $(s\Delta\theta/2)dg/d\eta$. The later follows from Eq. (17), or modified versions used elsewhere.[1] The values of the metastable minimum of $\Delta f(\eta)$ at $\eta=0$ increase with the magnitude of undercooling, $\Delta T \equiv T_M - T$, below the melting temperature T_M, and therefore the intercepts of $\sqrt{2\nu^2\Delta f}$ also increase with ΔT, as shown in Fig. 3. This figure depicts several situations that differ depending on the relative curvatures of the two integrands. At large undercoolings, $\Delta T_{\mathrm{large}}$, in the situation in Fig. 3(a), a *single intersection* exists at an η_{GB}^{eq} close to 1—predicting a relatively ordered GB. As supercooling decreases (increasing T), this intersection moves continuously towards a more disordered η_{GB}^{eq}. At the same time, with the y intercept of $\sqrt{2\nu^2\Delta f(\eta)}$ decreasing, the two curves come close to each other at low η_{GB} values. At decreased undercooling, ΔT_{med}, Fig. 3(a) illustrates the appearance of two additional equilibrium solutions characterized by smaller (i.e., more disordered) values of η_{GB}^{eq}.

When two additional intersections appear in Fig. 3(a), the middle intersection (i.e., the solution with a value between those of the relatively more ordered $\eta_{\mathrm{GB}}^{eq\text{-ord}}$ and more disordered $\eta_{\mathrm{GB}}^{eq\text{-dis}}$) is an unstable solution of η_{GB}^{eq}—it maximizes the area below the two curves. The remaining solutions, $\eta_{\mathrm{GB}}^{eq\text{-ord}}$ and $\eta_{\mathrm{GB}}^{eq\text{-dis}}$, are (meta)stable with stability rankings that depend on the hatched areas in Fig. 3(a) as discussed below. "Ordered" and "disordered" have relative meanings, since neither GB structure is purely crystalline nor liquidlike. Consideration of Eq. (11) shows that the disordered GB has a larger thickness because of its smaller lower integration limit.

When three intersections exist as in Fig. 3(a), their relative stability is graphically determined by considering their areas. For the leftmost ($\eta_{\mathrm{GB}}^{eq\text{-dis}}$) and rightmost ($\eta_{\mathrm{GB}}^{eq\text{-ord}}$) inter-

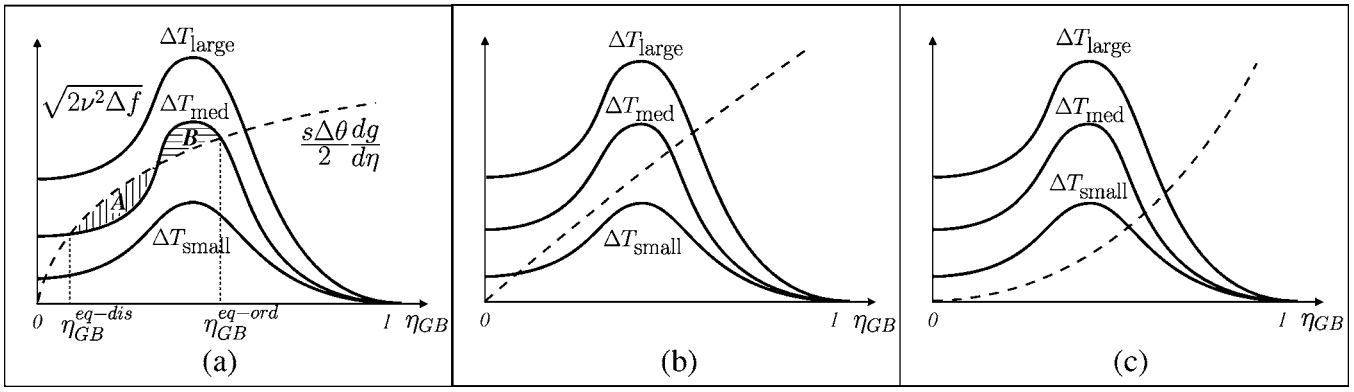

FIG. 3. Constructions depict differing GB transition behaviors for a range of undercoolings. The first frame, (a), illustrates the possibility of a first-order GB disorder transition below T_M. Frames (b) and (c) illustrate other types of GB behavior arising from changing curvature for the orientation gradient energy prefactor $g(\eta)$. In (b) only one solution exists that decreases continuously to $\eta_{\text{GB}}^{eq}=0$ as $T\rightarrow T_M$. In (c) only one solution exists, but has a limiting finite value, $\eta_{\text{GB}}^{eq}>0$, at $T=T_M$.

sections, the total area is equal to that below *all* segments of the two curves, plus the one hatched area that is opposite each specific intersection [i.e., plus area B in Fig. 3(a) for the $\eta_{\text{GB}}^{eq\text{-dis}}$ intersection and plus the area A for $\eta_{\text{GB}}^{eq\text{-ord}}$]. Thus, the intersection adjacent to the larger hatched area—area A in Fig. 3(a)—is the globally stable solution. The area associated with the middle intersection's solution is that under both curves plus both enclosed areas A and B; therefore it is greater than $\eta_{\text{GB}}^{eq\text{-ord}}$ or $\eta_{\text{GB}}^{eq\text{-dis}}$. As multiple intersections begin to develop, the area adjacent to the extant solution is initially the largest and subsequently decreases as the area associated with the metastable solution increases. Therefore, with decreased undercooling, the relative stability of the $\eta_{\text{GB}}^{eq\text{-ord}}$ and the $\eta_{\text{GB}}^{eq\text{-dis}}$ solutions may switch, with $\eta_{\text{GB}}^{eq\text{-dis}}$ becoming globally stable at the transition temperature for a given boundary. If the system parameters support such a switch, this temperature will characterize a first-order GB order-disorder structural transition. As undercooling is reduced further, $\eta_{\text{GB}}^{eq\text{-dis}}$ approaches zero, and the GB structure becomes liquidlike as the system approaches T_M. An additional aspect is that the solid-liquid energy barrier (in Δf) may become low enough so that the middle and right intersections will merge and disappear, as shown in Fig. 3(a), resulting in a loss of the $\eta_{\text{GB}}^{eq\text{-ord}}$ solution, and the only stable complexion just below T_M would be $\eta_{\text{GB}}^{eq\text{-dis}}$.

However, this sequence and the behavior with undercooling depend on the shapes of the two curves in Fig. 3. Two other modalities of GB behavior near T_M can be distinguished by increasing the curvature of $(s\Delta\theta/2)(dg/d\eta)$ relative to that of $\sqrt{2\nu^2\Delta f}$ or by varying the misorientation $\Delta\theta$. In Fig. 3(b), only one intersection, η_{GB}^{eq}, is generated, and it evolves continuously from $\eta_{\text{GB}}^{eq}\approx 1$ to $\eta_{\text{GB}}^{eq}\approx 0$ as $\Delta T\rightarrow 0$. In this case, there is no first-order GB transition below T_M, but the very small ΔT behavior is the same as for smaller (more negative) curvatures just described [viz. Fig. 3(a)]. This is the case of continuous GB disorder leading continuously to preferential melting. Figure 3(c) illustrates the third small ΔT modality. Again, a single intersection, η_{GB}^{eq}, is generated that decreases with decreasing ΔT, but its value remains finite as $T\rightarrow T_M$. In such systems, GBs are stable against *complete*, continuous preferential melting upon approach to T_M from below; moreover, they will not be perfectly wet by the liquid at equilibrium at T_M. [That $\eta_{\text{GB}}^{eq}\rightarrow 0$ corresponds to perfect wetting at T_M (i.e., $2\gamma_{\text{sol-liq}}=\gamma_{\text{GB}}$) will be justified below.]

Thus the three transition modalities have differing implications for macroscopic system behavior. The modalities can be cataloged based on two distinguishing phenomena: whether a first-order transition exists below T_M, and whether the GB is perfectly wet (i.e., $\eta_{\text{GB}}^{eq}\rightarrow 0$) at $T=T_M$. The particular behavior depends on the modeled system through the forms of $\Delta f(\eta;T)$ and $g(\eta)$ plus the values of gradient coefficients s and ν, and on the misorientation $\Delta\theta$. How $\Delta\theta$ affects GB behaviors is of particular interest because it will vary from boundary to boundary in a polycrystal while the others are "system parameters" fixed by the material. An extended graphical analysis of misorientation effects and also of these system parameters follows.

By inserting the leading behavior for $g(\eta)$ from Eq. (17), Eq. (14) becomes

$$[\Delta f(\eta_{\text{GB}}^{eq})]^{\beta}=\alpha\eta_{\text{GB}}^{eq}, \tag{18}$$

where

$$\beta=\frac{1}{2(p-1)},\quad \alpha=\left(\frac{sp}{2\sqrt{2}\nu}\Delta\theta\right)^{2\beta},\quad p>1. \tag{19}$$

Equations (17) and (18) permit a general graphical construction for η_{GB}^{eq} by plotting the two sides of Eq. (18) against η.

In Eq. (18), the g-dependent curve is a straight line that passes through the origin with a slope α proportional to $(\Delta\theta)^{2\beta}$, and the homogeneous free-energy curve is a double-well function raised to a power β.

For a given system, the range of GB misorientations is represented by a fan of lines emanating from the origin. For the case illustrated in Fig. 4(a), when there is at least one boundary misorientation that produces three intersections with $[\Delta f(\eta)]^{\beta}$ below T_M, two bounding tangent lines, associated with an upper $\Delta\theta_U$ and a lower $\Delta\theta_L$ misorientation, are produced by the fan. (It is assumed for this demonstration that both $\Delta\theta_U$ and $\Delta\theta_L$ lie within the range of allowable misorientations which would be $0<\Delta\theta<2\pi$ with low-symmetry crystals and reduced by additional crystal symme-

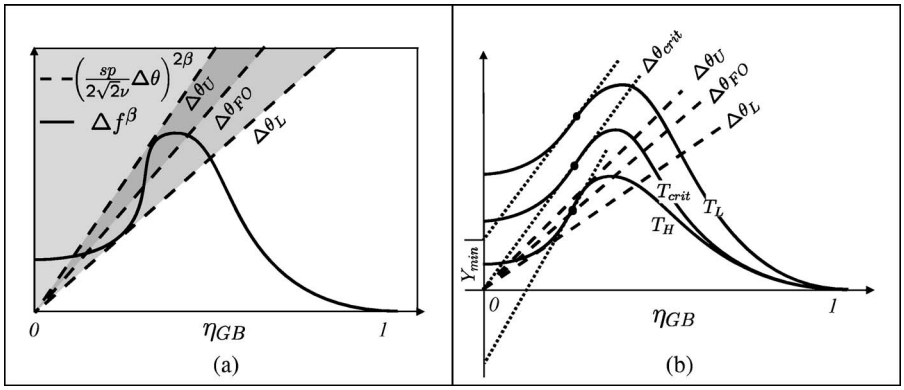

FIG. 4. Extended construction to reveal behavior as a function of GB misorientation. (a) The $\Delta\theta_U$ and $\Delta\theta_L$ define upper and lower bounds to a fan of lines for those $\Delta\theta$ having three intersections. Frame (b) illustrates how the sign of the y-axis intercept, Y_{min}, of the tangent line of the nearest inflection point of $[\Delta f(\eta)]^{\beta}$ evolves with temperature. No first-order transition at any GB is possible when Y_{min} is positive.

try.) Any misorientation $\Delta\theta_L<\Delta\theta<\Delta\theta_U$ will have two (meta)stable GB structures at the given ΔT. A particular $\Delta\theta_{FO}(T)$ that has the equilibrium first-order transition at the temperature for which the plot is obtained separates the fan into an upper region, wherein $\eta_{\mathrm{GB}}^{eq\text{-dis}}$ is globally stable, and a lower region, where $\eta_{\mathrm{GB}}^{eq\text{-ord}}$ is globally stable.

However, the two tangent lines of $(\Delta f)^{\beta}$ that define $\Delta\theta_U$ and $\Delta\theta_L$ may not exist at all temperatures. To establish a criterion for their existence, consider the first inflection point of $(\Delta f)^{\beta}$ (i.e., the inflection with the smallest η value). Of all the tangent lines from $(\Delta f)^{\beta}$, the one at this point yields the smallest y-intercept value Y_{min} [as drawn in Fig. 4(b)]. (The $\eta=0$ intercept is $Y(\eta)=[\Delta f(\eta)]^{\beta}-\eta\partial\Delta f^{\beta}/\partial\eta$ for a line tangent to Δf^{β} at η. Extreme values of $Y(\eta)$ determined by $Y'=0$ occur at any inflection point of $(\Delta f)^{\beta}$ where $\eta\neq 0$.) No tangent lines can pass through the origin if $Y_{min}>0$. However, two such lines ($\Delta\theta_U$ and $\Delta\theta_L$) do exist if $Y_{min}<0$, which is a necessary condition for a first-order GB order-disorder transition to occur.

In some systems, a critical temperature can be defined for an undercooling ΔT_{crit} where $Y_{min}=0$, as illustrated in Fig. 4(b). Then, for $T<T_M-\Delta T_{crit}$, Y_{min} will be positive and no first-order transition will appear for *any* misorientation angle. At $T=T_M-\Delta T_{crit}$, only that tangent line for the first inflection crosses the origin. The slope of that tangent line defines a critical misorientation, $\Delta\theta_{crit}$. Misorientations of $\Delta\theta>\Delta\theta_{crit}$ will always have greater values than $\Delta\theta_U(T)$ at temperatures $T>T_M-\Delta T_{crit}$. Therefore, the dashed lines in Fig. 4 for $\Delta\theta>\Delta\theta_{crit}$ have only one intersection with Δf^{β} which approaches the origin as $\Delta T\to 0$ (i.e., $\eta_{\mathrm{GB}}^{eq}\to 0$). Their associated complexions thus will exhibit continuous melting and have perfect wetting behavior (as elaborated below). For misorientations just less than $\Delta\theta_{crit}$, three intersections will appear above $T-\Delta T_{crit}$, and a first-order GB transition is possible when $\Delta\theta\geqslant\Delta\theta_{FO}(T)$. Finally, when $\Delta\theta$ is less than $\Delta\theta_{FO}(T)$ below T_M, there is only one intersection and it remains at a finite η_{GB}^{eq} value as $T\to T_M$. Such GBs will not be fully disordered nor wet by liquid at T_M.

Plotting the three characteristic misorientation angles, $\Delta\theta_{FO}$, $\Delta\theta_L$, and $\Delta\theta_U$, against temperature yields three curves on the T-$\Delta\theta$ plane forming an interfacial complexion diagram. These lines represent the first-order GB order-disorder transition line and the two metastable existence limits. The three lines terminate at the critical point $(T_{crit},\Delta\theta_{crit})$, as shown in Fig. 5. The critical conditions, $(T_{crit},\Delta\theta_{crit})$, are determined from the construction by

$$0=[\Delta f(\eta_{crit};T_{crit})]^{\beta}-\eta_{crit}\left.\frac{\partial\Delta f^{\beta}}{\partial\eta}\right|_{\eta_{crit},T_{crit}},$$

$$0=\left.\frac{\partial^2\Delta f^{\beta}}{\partial\eta^2}\right|_{\eta_{crit},T_{crit}},$$

$$\Delta\theta_{crit}=\frac{2\sqrt{2}\nu}{sp}\left(\left.\frac{\partial\Delta f^{\beta}}{\partial\eta}\right|_{\eta_{crit},T_{crit}}\right)^{1/2\beta}. \tag{20}$$

Within the limits of the metastable existence curves in Fig. 5, both the ordered and disordered configurations can exist in (meta)stable equilibrium, whereas outside these limits only one complexion exists. The complexions may coexist stably only at temperatures and misorientations indicated by the first-order transition curve.

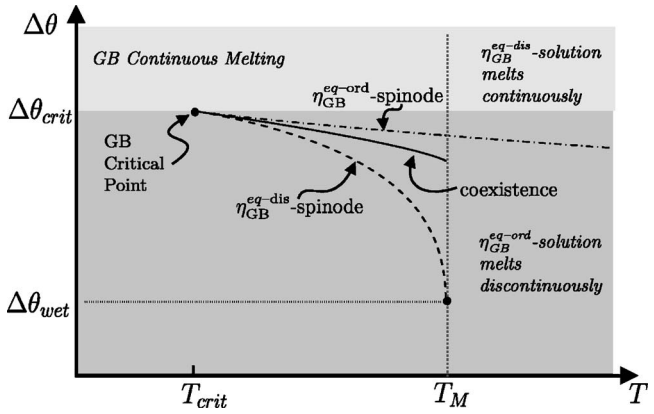

FIG. 5. An example of a GB-complexion diagram (the interface equivalent of a phase diagram) for a system that admits a first-order interfacial transition. The solid curve delineates first-order grain boundary transitions—on the low T and $\Delta\theta$ side, the more ordered complexion ($\eta_{\mathrm{GB}}^{eq\text{-ord}}$) is more stable, while the more disordered complexion ($\eta_{\mathrm{GB}}^{eq\text{-dis}}$) is more stable on the other side. The first-order curve terminates at a critical point $(T_{crit},\Delta\theta_{crit})$ at which the transition is higher order. The dashed curves indicate existence limits (spinodes) for the metastable extensions of the $\eta_{\mathrm{GB}}^{eq\text{-ord}}$ solution (upper, dash-dotted curve) and $\eta_{\mathrm{GB}}^{eq\text{-dis}}$ solution (lower, dashed curve). The extension of the $\eta_{\mathrm{GB}}^{eq\text{-ord}}$ spinode to $T>T_M$ indicates whether an ordered GB could metastably superheat.

Finally, if $Y_{min} \geq 0$ for all $T \leq T_M$, multiple intersections will not be generated, and the three lines will not appear as in Fig. 5. In this case, GBs will have continuously increasing disorder up to $T=T_M$.

As $T \rightarrow T_M$, the asymptotic behavior of GBs can be analyzed by expanding $\Delta f(\eta;T)$ about $\eta=0$ and $T=T_M$:

$$\Delta f(\eta) \approx \frac{\Delta h_M}{T_M}\Delta T + A\eta^q, \tag{21}$$

where $\Delta T = T_M - T$ is the small undercooling, Δh_M is the melting enthalpy per volume, A is a positive constant, and q is greater than 1. Using Eq. (17) for $g(\eta)$, Eqs. (14) and (21) give

$$\frac{\Delta h_M}{T_M}\Delta T + A\eta^q \approx \left(\frac{sp}{2\sqrt{2}\nu}\Delta\theta\right)^2 \eta^{2(p-1)}. \tag{22}$$

Equation (22) implies that, for both stable and metastable disordered GBs, η_{GB}^{eq} goes continuously to zero as $\Delta T^{1/(2p-2)}$ when $1 < q/(2p-2)$. When $1 = q/(2p-2)$, complete melting also occurs, but only for GBs with $\Delta\theta > \Delta\theta_{wet} = 2\nu\sqrt{2A}/sp$. When $q/(2p-2) < 1$, there is no solution to Eq. (22) at $\eta \approx 0$ because the left-hand side always exceeds the right when η is sufficiently small. For this case, η_{GB}^{eq} remains finite at T_M, which infers unconditionally that complete GB premelting at T_M does not occur for any $\Delta\theta$, nor does perfect liquid wetting.

The asymptotic behavior of the GB thickness can be obtained from Eq. (11) by assuming a fixed η value (near 1) specifies the edge of the GB core. The thicknesses of disordered GBs always diverge as $T \rightarrow T_M$. However, the divergence rate is either logarithmic for $q=2$ or obeys a power law relationship for $q>2$,

$$W_{\mathrm{GB}} \sim \begin{cases} \ln(T_M/(T_M - T)), & q = 2, \\ ((T_M - T)/T_M)^{1/q-1/2}, & q > 2. \end{cases} \tag{23}$$

The logarithmic divergence of film thickness for $q=2$ is a typical result of mean field theories, and it agrees with the results of other modeling methods.[6,28,62] The logarithmic divergence results from a Δf that is quadratic near $\eta=0$. However, in one MD study it was noted that the widths could fit $(\Delta T)^{-1/4}$,[62] which would agree with the above relation for $q=4$.

The above analysis establishes that, as $T \rightarrow T_M$, a disordered GB with vanishing η_{GB}^{eq} widens due to the gradient penalties. The misorientation penalty disappears as the boundary thickness increases. In this limit, Eqs. (5) and (13) become

$$\frac{\gamma_{\mathrm{GB}}}{2} = \gamma_{sl} = \int_0^1 \sqrt{2\nu^2 \Delta f(\eta, T_M)}\, d\eta, \tag{24}$$

which is the solid/liquid interfacial energy at T_M.

Thus, any disordered GB that premelts upon approach to T_M is also perfectly wet by the equilibrium liquid at T_M. On the other hand, ordered GBs have a finite η_{GB}^{eq} at T_M and are not perfectly wetted. For this reason, $\Delta\theta_L(T_M)$ corresponds to $\Delta\theta_{wet}$, the wetting transition misorientation, as in Fig. 5.

A perfect solid can be superheated in the absence of liquid nucleation. The free surface provides barrierless nucleation if the liquid perfectly wets the solid surface. Not all crystal surfaces are perfectly wet by their equilibrium melt at $T=T_M$; pure Pb is an example.[13] Grain boundaries will also provide nucleation sites, and their wetting behavior will determine whether a solid can be superheated in the absence of free surface nucleation, or suppress superheating and promote melting, especially for confined solids with no free surfaces. To analyze superheated GBs, the complexion diagram can be extended to temperatures above T_M using the graphical analysis. Figure 5 shows that, of the three characteristic lines, only the $\eta_{\mathrm{GB}}^{eq\text{-ord}}$ curve extends above T_M. The $\eta_{\mathrm{GB}}^{eq\text{-dis}}$ complexion (liquid in this case) is more stable than the $\eta_{\mathrm{GB}}^{eq\text{-ord}}$ complexion for all $T>T_M$, but the ordered GB is metastable for $\Delta\theta < \Delta\theta_U$ and will melt given a nucleation event. The $\eta_{\mathrm{GB}}^{eq\text{-ord}}$ complexion is unstable for $\Delta\theta > \Delta\theta_U$ above T_M.

IV. NUMERICAL EXAMPLES

Our first numerical example uses the following model,

$$\Delta f(\eta) = \frac{\Delta h_M}{T_M}(T_M - T)(1-\eta)^3(1 + 3\eta + 6\eta^2) + \frac{a^2}{2}\eta^2(1-\eta)^2 + \frac{b^2}{2}\eta^4(1-\eta)^4,$$

$$sg(\eta) = s\eta^2. \tag{25}$$

The first term of Δf approximates a step function that decreases from $(\Delta h_M/T_M)(T-T_M)$ to 0 at $\eta=\frac{1}{2}$; the second and third terms simulate an energy barrier between liquid and crystalline states.

The calculation of η_{GB}^{eq}, the GB energy, and thickness follows Eqs. (11), (13), and (14). The GB thickness is calculated by setting the edge of GB core at $\eta=0.9$. The model can be scaled and the only significant parameter is the b/a ratio. Figure 5 is the calculated GB phase diagram for this model when $b/a=10$ [in Fig. 5 the coordinate labels are omitted but they are $(\Delta h_M \Delta T/(a^2 T_M), s\Delta\theta/(a\nu))$]. The first-order GB transition line and the two metastable GB-phase existence limits in Fig. 5 terminate at a critical point $(\Delta h_M \Delta T_{crit}/(a^2 T_M), s\Delta\theta_{crit}/(a\nu)) = (0.0148, 1.722)$. The GB energy and thickness are plotted in Figs. 6(a) and 6(b) for several misorientations as functions of temperature. First-order and continuous GB transitions are exhibited for two of the larger misorientations. Their thicknesses diverge as $\log[T_M/(T_M - T)]$, consistent with Eq. (23), and their energies are twice the liquid/solid interface energy at T_M. The GB with a smaller misorientation has finite thickness at T_M and its energy is less than $2\gamma_{sl}$.

In previous simulations of KWC, the $\eta^4(1-\eta)^4$ term in Δf was absent from Eq. (25) ($b=0$). Its absence gives a liquid/solid energy barrier that is less steep than the present model and produces the result that the three characteristic lines in Fig. 5 shrink to a single critical point at $(T_M, \Delta\theta_{crit} = a\nu/s)$. In this case, a GB either has no transition below T_M

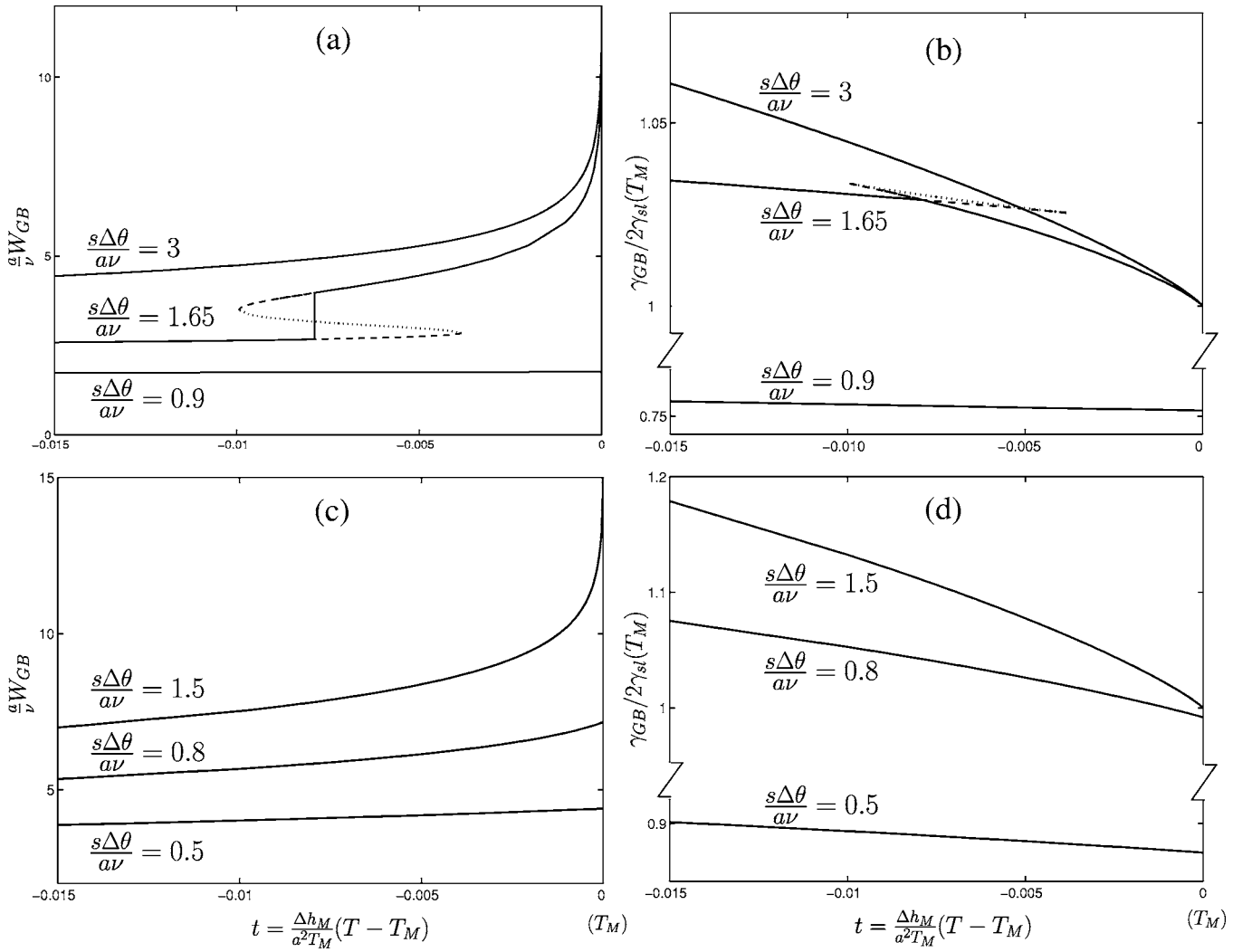

FIG. 6. Normalized grain boundary thicknesses and energies as functions of reduced temperature and misorientation for two models of Δf. The GB thicknesses are normalized with ν/a, and GB energies normalized with $2\gamma_{sl}$ (i.e., twice the solid/liquid interface free energy at T_M). γ_{sl} is calculated as $\int_0^1\sqrt{2\nu^2\Delta f(\eta,T_M)}d\eta$. In (a) and (b), small $\Delta\theta$ shows limited disorder up to T_M, intermediate $\Delta\theta$ exhibits a first-order transition, and large $\Delta\theta$ continuously premelts. The (c) and (d) frames illustrate how reduced barrier steepness [the $b=0$ case in Eq. (25)] moves the critical point to T_M and thereby eliminates the first-order transition from the complexion diagram. The dashed lines represent metastable extensions of ordered and disordered GBs. The dotted lines represent the unstable solution.

when $\Delta\theta<\Delta\theta_{crit}$, or undergoes a continuous melting for $\Delta\theta>\Delta\theta_{crit}$. The first-order GB transitions were not observed in simulations for $b=0$.[49,50] The GB energies and thicknesses for the $b=0$ model are plotted in Fig. 6 for comparison.

The Δf and $g(\eta)$ can be generalized to

$$\Delta f(\eta)=\frac{\Delta h_M}{T_M}(T_M-T)(1-\eta)^3(1+3\eta+6\eta^2)+\frac{a^2}{32}[4\eta(1-\eta)]^q,\quad q\geqslant 2.$$

$$sg(\eta)=s\eta^p,\quad p>1, \tag{26}$$

which produces a model that depends on the choice of p and q. It becomes the previous model with $b=0$ when $p=q=2$. At the melting point, Eq. (18), which determines equilibrium GB states, becomes

$$[4\eta_{\mathrm{GB}}(1-\eta_{\mathrm{GB}})]^{q/(2p-2)}=\left(\frac{4ps\Delta\theta}{\nu a}\right)^{1/(p-1)}\eta_{\mathrm{GB}}. \tag{27}$$

Figure 7 shows how Eq. (27) depends on the value of $q/(2p-2)$.

For $q/(2p-2)>1$, the slope of the left-hand side of Eq. (27) is 0 at $\eta_{\mathrm{GB}}=0$. $\eta_{\mathrm{GB}}=0$ is always a (meta)stable solution of Eq. (27) as judged by either Eq. (16) or from graphical analysis. Therefore, all GBs are wetted by liquid at the melting point in this case and $\Delta\theta_{wet}\rightarrow 0$ in Fig. 5. However, some misorientations may produce three intersections (e.g., $\Delta\theta_1$ in Fig. 7) while others produce only one (e.g., $\Delta\theta_2$). Therefore, complete GB wetting can be produced continuously or by a first-order transition.

For $q/(2p-2)<1$, the slope of the left-hand side of Eq. (27) is ∞ at $\eta_{\mathrm{GB}}=0$, and $\eta_{\mathrm{GB}}=0$ is an unstable solution for all

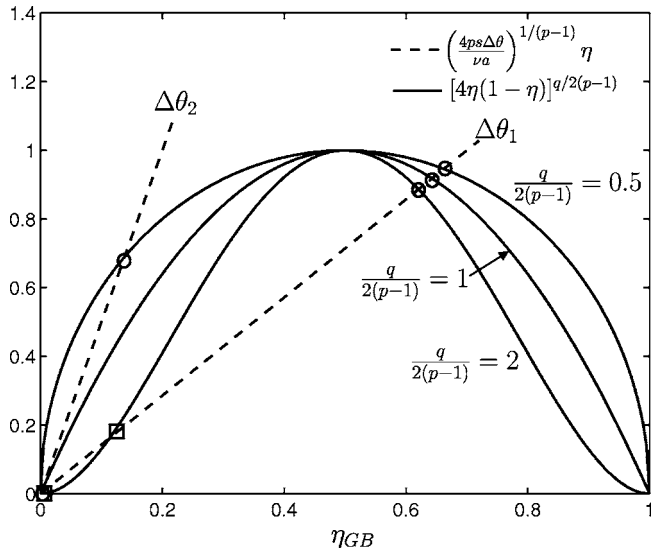

FIG. 7. Specific examples of three characteristic shapes of $\Delta f(\eta, T_M)^{\beta} \propto [4\eta(1-\eta)]^{q/(2p-2)}$ that cause different limiting behavior as $T \to T_M$. Intersections with the straight lines define the behavior of GBs. Three different types of wetting behavior emerge depending upon the types of intersections possible. For $q/(2p-2) > 1$, first-order or continuous disorder transitions lead to complete GB wetting at T_M for all $\Delta\theta$. For $q/(2p-2)=1$, complete GB wetting can result for $\Delta\theta \geqslant \Delta\theta_{wet}=(\nu a)/s$, but not for $\Delta\theta < \Delta\theta_{wet}$. For $q/(2p-2)<1$, every GB will have limited disorder at T_M, and the liquid will not perfectly wet its equilibrium solid phase. The intersections with circle markers represent local energy minima. Those with square markers are local maxima.

$\Delta\theta$. Therefore, no GB is wetted by a liquid at T_M and there is no GB transition at any $\Delta\theta$ below T_M.

The intermediate case, $q/(2p-2)=1$, has a finite slope in Fig. 7. The $\eta_{\mathrm{GB}}=0$ is a stable solution for $\Delta\theta > \nu a/s$ (e.g., $\Delta\theta_2$) but not stable at smaller misorientations (e.g., $\Delta\theta_1$). Complete wetting only occurs at GBs with misorientations larger than $\nu a/s$.

Therefore, the phenomenon of complete GB wetting at T_M and GB transitions below T_M can be predicted from the ratio of $q/(2p-2)$. This is in agreement with the GB asymptotic behavior analysis in the previous section.

V. DISCUSSION

Our results predict that grain boundaries will have an equilibrium complexion selected from a spectrum of disordered structures. The tendency to disorder increases with misorientation and with temperature up to the melting point where the crystal stably coexists with a completely disordered (e.g., liquid or amorphous) structure. These results can be understood heuristically if the energy increase resulting from a layer of nonequilibrium bulk material is compensated by an energy decrease obtained by converting an ordered grain-boundary interface into two lower energy interfaces. This observation suggests that a continuous increase in grain boundary width and disorder as $T \to T_M$ could be considered a "premelting" localized at those grain boundaries with sufficiently large defect energies.

Moreover, the model identifies the conditions that some materials systems will possess first-order transitions between disordered complexions at a specific curve in misorientation-temperature space. Figure 5 is a grain-boundary complexion diagram that indicates the temperatures and misorientations where two types of grain-boundary "phases" exist as a stable or a metastable complexion. The curve at which complexions co-exist at equilibrium is analogous to that in Cahn's CPWT phase diagram:[2] η_{GB}^{eq} is analogous to Γ_B^{eq} which also has two coexistant equilibrium values for which the difference vanishes at a critical point. This similarity is inevitable because KWC and CPWT have isomorphic free energy functionals [Eqs. (5) and (6)]. However, in this model, the interface term $s\Delta\theta g(\eta_{\mathrm{GB}})$ is derived from a GB functional in Eq. (1).

In this model, no special misorientations are associated with cusps in $\gamma_{\mathrm{GB}}(\Delta\theta)$ (except at $\Delta\theta=0$) that have been observed elsewhere (e.g., Refs. 63–66). Including multiple cusps in a KWC model would be possible through modification of the $|\nabla\theta|$ term in Eq. (1) with a function $t(|\nabla\theta|)$ that has multiple minima. Furthermore, this model does not provide an upper bound for misorientation—$\Delta\theta$ can be at most 2π in crystals with the lowest possible symmetry, and this upper bound will be smaller in most systems of interest. Therefore, in practice, complexion diagrams will be restricted to lower subregions of Fig. 5 and the curve of first-order transitions may intersect—and thus terminate without a second-order transition—at the maximum allowed misorientation.

Polycrystalline materials will typically contain grain boundaries with all possible misorientations; therefore, at a fixed temperature, observable complexions would range over those which appear along a constant temperature (vertical) line in Fig. 5. However, microstructural evolution or texture affect the distribution of GB misorientations, and the frequency of observed complexions may not be directly related to their relative line intersection lengths. The behavior of a fixed polycrystalline microstructure may have a complex temperature relationship: some grain boundaries may have continuous or first-order premelting behavior until the grain boundary is replaced with a perfectly wetting liquid at $T=T_M$; others could remain ordered without nucleating a more disordered complexion as $T \to T_M$. The ranges of misorientations for which these behaviors are possible are separated by the values of $\Delta\theta$ where the curves for the two spinodes and the first-order transitions intersect the line $T=T_M$.

Specific composition diagrams can be obtained numerically for particular models of free energy, Δf, and misorientation gradient penalty. The manner through which Δf and $g(\eta)$ combine to create a spectrum of diagrams were explored by developing a test model that depends on a ratio $q/(2p-2)$ relating the steepness of the misorientation penalty [via q in Eq. (25)] to Δf [via p in Eq. (17)]. This generic model could also serve as a foundation upon which material-specific models for p and q could be tuned by comparing model predictions to empirical observation. However, such a tuning scheme would not serve as an independent verification of this model. Preferably, those continuum-model parameters which cannot be obtained through direct observation could be obtained through coarse-graining of atomistic

simulation data (e.g., the decaying length of solid-liquid interface observed in MD and classical density functional theory).

Some corroborative evidence for the qualitative behavior of the model presented in this paper can be obtained by comparison to published atomistic grain boundary simulations. Molecular dynamics simulations of metallic grain boundaries have demonstrated that grain boundary cores tend to disorder with increasing temperature and that this tendency is increased for larger misorientations.[66,67] Considering that a fixed $\Delta\theta$ requires that a grain boundary system must promote collective bond distortion, this trend could be rationalized through the thermodynamic consideration of entropic and enthalpic differences between ordered grain boundary cores with overlapping elastic fields and disordered cores with reduced elastic energy densities. Such considerations are consistent with the form of Eq. (1); in fact, it is possible to modify $g(\eta)$ so that γ_{GB} is the Read-Schockley form derived from interacting dislocations at small misorientations.[1]

Molecular dynamic determination of bulk melting temperature is troublesome and incurs errors of at least a few percent.[33,34,37] Consequently, molecular dynamic confirmation of grain boundary transitions, such as premelting, is difficult and more uncertain. Structural fluctuations and stochastic grain boundary migration can be misinterpreted as evidence of a complexion transition. We have no estimates of the values for nucleation barriers to complexion transitions which could be used to estimate the duration of an MD simulation which might produce them. Furthermore, characterization is hindered by the absence of a standard measure for local disorder, such as η. Moreover, the complexion diagram's sensitivity to model parameters [such as p and q in Eqs. (25) and (17)] may indicate a similar sensitivity of atomistic simulations to models of interatomic potentials. Systems that are likely candidates for complexion transitions (i.e., those that form glasses, have complex grain boundary structures, or highly-populated unit cells) are probably the most difficult to subject to reliable MD simulations.

Nevertheless, extant simulations do provide evidence that premelting occurs for higher-energy GBs. Simulations on tilt boundaries have demonstrated increasing disorder and characterized divergent grain boundary widths as $T \rightarrow T_M$.[6,28,62] In other simulations, tilt and twist boundaries exhibited wide disordered structures at $0.98T_M$, but the T_M asymptotic behavior was not characterized.[40,68,69] In Si simulations, low-angle twist boundaries (about [111]) remained narrow and crystalline at $0.95T_M$, but higher-energy density GBs show increasing disorder with T.[31,70] However, other simulations report that these boundaries remain narrow and retain some of crystallinity at $0.95T_M$.[33,34]

Molecular dynamics evidence for first-order grain boundary transitions is often indirect. In one MD study, high-energy GBs clearly disordered below T_M; at T_M, low $\Delta\theta$ remained structurally *stable*, and intermediate cases exhibited ranges of disorder.[62] Several MD and Monte Carlo studies found two or more GB metastable configurations for the same boundary at fixed temperature.[35,40–44]

Other indirect evidence is available from simulations of temperature-dependent grain boundary properties. Simulations of GB migration and diffusion in fcc metals suggest discontinuous reductions in activation energies at $(0.6-0.8)T_M$ and may indicate a first-order GB transition.[45–47] Futhermore, atomic displacements within the GB core become more isotropic above the transition which is consistent with a more disordered GB structure.[45,46]

In experiments and simulations, there may be a bias towards special boundaries that have higher symmetry and lower energy than random boundaries and towards materials that do not easily form glass. Such a bias would tend to underrepresent observations of complexion transitions suggested by Fig. 7.

Interpretation of reported TEM evidence is also nontrivial. First, absence of observation does not imply absence of phenomenon; transitions tend not to occur at the lower end of the grain boundary energy spectrum. Second, presumptions that premelting must result in a completely amorphous core may have led researchers to neglect observations of partially ordered GBs. The structural difference between ordered and disordered GBs could be subtler and harder to discern than expected. To be observed in the best conditions, a disordered region must be several atomic layers thick.

However, an *in situ* TEM study of a Bi tilt boundary near T_M showed the dihedral angle, ψ, where a GB intersects solid/liquid interface, decreased with increasing $\Delta\theta$, and ψ dropped discontinuously to zero at $\Delta\theta=15°$.[27] One interpretation is that the GB energy was discontinuous at $\Delta\theta=15°$, but this is puzzling for complete equilibrium. It may be indicative of a first-order transition allowing coexistence of metastable GB complexions.

Because free-surface premelting is a similar, and a perhaps related, phenomenon, it is instructive to consider the requirements for its observation at the surfaces of pure metals. Premelting of various metallic surfaces has been observed with melted layer widths of approximately five monolayers at $T_M-T=1°$ characterized by $\ln[T_M/(T_M-T)]$.[18,19] That premelting is only observed in TEM observations of Al GBs above $0.999T_M$ (Ref. 26) is qualitatively consistent with surface premelting observations. Metallic free surfaces exhibit about one monolayer of disorder that develops more than 10° below T_M.[18,19]

At $0.5-0.9T_M$, some metallic free surfaces can have roughening transitions[15] where ledges and kinks disorder. For grain boundaries well below T_M, comparable phenomena are that the population of point defects and dislocations in the core's vicinity increases with temperature. TEM observations showed that secondary GB dislocations in pure Al persisted to $0.96T_M$.[26,71] Observations show that particle rotations which are driven by grain boundary anisotropy persist up to $0.96T_M$ and $0.99T_M$ in Cu and Ag.[72,73] Both observations indicate that some boundary-core coherency remains even though they may premelt closer to T_M. It is also known that roughening (also known as defaceting) transitions of faceted GBs in pure metals occur at $0.6-0.9T_M$ (Refs. 74 and 75), suggesting that the resultant stable general GBs are more disordered than the lower-temperature faceted GBs.

Our model does not include effects of dispersion forces on GB structure and width (most atomistic simulations also disregard these forces). Although they are small in comparison to forces that directly affect bonding, dispersion forces are known to be repulsive in premelted surface layers and in-

crease layer width.[18] Because the core of a GB is probably less dense, GB dispersion forces will be attractive GB.[76] For an ordered GB in $SrTiO_3$, the dispersion energy accounts for $\sim 5\% - 10\%$ of the total binding energy.[77]

Our model suggests that it may be possible to superheat the metastable $\eta_{\mathrm{GB}}^{eq\text{-ord}}$ solution above T_M in Fig. 5 for grain boundaries with $\Delta\theta < \Delta\theta_U$. This can be compared to melting at free surfaces, at which detectable superheating is rare. In rare cases, for example Pb(111) and Ge(111), surfaces exhibit some disorder but do not fully premelt.[14,78] Moreover, not all Pb surfaces are wet by the pure liquid at T_M.[13] Recently it was shown that these highly ordered surfaces could be flash heated to $1.15T_M$ without fully disordering—suggesting first-order transition behavior.[79,80]

Of the three transition modalities depicted in Fig. 5, the two spinodals pertain for metastable behavior at $T > T_M$. The higher of the two, $\Delta\theta_U(T)$, is the stability limit for ordered complexions. At $T > T_M$, a GB with $\Delta\theta > \Delta\theta_U$ will spontaneously disorder as quickly as interfacial kinetics permit—it cannot be further superheated. However, GBs that have a metastable $\eta_{\mathrm{GB}}^{eq\text{-ord}}$ structure ($\Delta\theta < \Delta\theta_U$) could be superheated; solids containing only such GBs thus could be superheated metastably until a nucleation event occurs. However, we expect that triple junctions would provide heterogeneous nucleation sites or would melt spontaneously. The other spinodal, $\Delta\theta_L(T)$, goes to $\Delta\theta = 0$ at $T \geqslant T_M$; thus the more stable $\eta_{\mathrm{GB}}^{eq-\mathrm{dis}}$ solution allows barrierless melting. Simulations of superheated Si and metallic grain boundaries showed that GBs directly disordered, and the liquid band grew as fast as interfacial kinetics allowed.[33,34,37] We suggest that GBs that melted without incubation above T_M (Refs. 33, 34, and 37) would completely premelt as $T \to T_M$. This is based on observation that the same simulations showed that melting at low-energy free-surface orientations *did* require incubation at $T > T_M$.

Thus, we suggest that the general predictions of GB disorder made in this paper, including the possibility of a first-order transition in boundary structures, is not inconsistent with published TEM and simulation evidence. Verification of the existence of partially ordered grain boundaries and their transitions, or a demonstration of their absence, constitutes a challenge to the TEM and simulation communities.

If metallic systems are not ideal for the observation of GB structural transitions, which systems would be better? GB disorder is promoted in materials where the molar free energy difference between crystalline and liquid states is small. Systems with short-range order in their liquid phase, as with liquid silicates, will have larger atomic complexes which participate in disorder, so disordered boundary cores will be widened and thus easier to see. The gradient coefficient s should probably increase with the length scale of short-range order. Increased energy barrier height in Δf permits greater undercooling for stabilized disorder GBs (as in Fig. 6) and premelted GB films should occur over a wider temperature range in good glass formers. Polymeric systems, particularly semi-crystalline polymers, polycrystalline metals that readily form bulk-metallic glasses, and liquid crystals are candidates.

Finally, sure evidence of GB structural transitions exists for multicomponent ceramic systems. Nanometer thick, equilibrium films, rich in SiO_2 or Bi_2O_3, comprise the GBs in various ceramics.[53,54,81–83] Such films have thicknesses that depend on the additive chemical potential,[53,54,81,82,84] distinct compositions compared to those of the bulk liquid phases present,[53,83–87] and exhibit thermodynamic stability.[52–54,82–84] We propose that such intergranular amorphous films are a high-temperature GB complexion resulting from a coupled prewetting/premelting transition. In addition, considerable evidence from kinetic behavior points to the existence of GB transitions yielding similar GB structures in multicomponent metallic systems.[51,55,57,58] This view is supported by a similar analysis of the KWC model extended to binary systems (yet to be published).

VI. CONCLUSIONS

The KWC diffuse interface model for grain boundaries predicts disorder transitions. The model predictions of disordered GB core material can be associated with the appearance of a liquid phase, and therefore this diffuse interface model can be considered a premelting theory for grain boundaries as a function of their misorientation. The graphical construction for equilibrium grain boundary properties can be used to construct a "grain boundary complexion diagram" that predicts which of two more and less ordered grain boundary structures would be most stable for values of temperature and misorientation. The model predicts the possibility that first-order transitions between a more ordered and a less ordered grain boundary structure can occur with increasing temperature below the melting temperature. The types of grain boundary structures and the temperature behavior for transitions between the structures will directly affect macroscopic material properties, such as creep and grain boundary migration, for polycrystals. The features on the GB complexion diagram depend on the homogeneous free energy density for the crystalline and noncrystalline fixed stoichiometric material and on models for energy penalties for inhomogenous distributions of disorder and crystallographic orientation. The diagram's possible features are (1) the critical point's location $(T_{\mathrm{crit}}/T_M, \Delta\theta_{\mathrm{crit}})$, (2) a spinodal curve for the upper stability limits for the more disordered structure, (3) a spinodal curve for the lower stability limits for the less disordered structure, and (4) the upper limit to grain boundary misorientations with equilibrium structures that do not perfectly wet the boundary at T_M. Not all features will appear on a given complexion diagram, as illustrated and predicted from a quantitative measure $q/(2p-2)$ of power law approximations to the free energy density (q) and the disorder dependence of gradient coefficient function for misorientation (p).

Along with premelting behavior, extensions of the model above the melting point show that, when the equilibrium structure perfectly wets its grain boundary, no barrier to melting occurs at $T \geqslant T_M$. However, low misorientation boundaries in some material systems can have nonperfectly wetting metastable structures that could be superheated absent a finite nucleation event.

Some experimental observations and some atomistic simulations have qualitative behaviors that are consistent

with the model's predictions. A subset of these simulation models has some quantitative measure that could be used to calibrate model parameters. However, the absence of standard methods to characterize a continuum of disorder from collections of atomic positions from simulation data or from diffraction data make direct model verification difficult. Characterization of continuous spatial distributions of order is a challenge for materials simulators, theorists, and experimentalists.

ACKNOWLEDGMENTS

The work of M.T. and W.C.C. was supported by NSF Grant No. DMR-0010062. R.M.C. was supported by the Office of Basic Energy Science, Division of Materials Sciences and Engineering of Department of Energy under Contract No. DE-AC03-76F00098. The work described here was conducted in cooperation with the whole NANOAM collaboration whose European partners were funded from EU Commission Contract G5RD-CT-2001-00586. Discussions with Dr. J.A. Warren and Dr. C.M. Bishop are gratefully acknowledged. We also acknowledge useful comments from the anonymous reviewers.

APPENDIX

For a plausible, but untested, example, a local crystallinity measure might be defined by an atom's (located at $\vec{\zeta}$) radial distribution function $\alpha_{\mathrm{rdf}}(\vec{x}-\vec{\zeta})$,[88] or its bond-angle distribution function $\alpha_{\mathrm{bda}}(\vec{\zeta})$,[89,90] or the ratio (surface area)/(volume)$^{2/3}$ of its Voronoi tessellation, α_{V}.[89] In each case, a distance metric $\langle,\rangle$ [i.e., $\langle\alpha(\vec{\zeta}),\alpha^{\mathrm{xtal}}\rangle$ that scales with the departure from an ideal crystal, and $\langle\alpha(\vec{\zeta}),\alpha^{\mathrm{amorph}}\rangle$ for an amorphous structure] could be defined and for each atom

$$\eta(\vec{\zeta}) \equiv \left(\frac{\langle\alpha(\vec{\zeta}),\alpha^{\mathrm{amorph}}\rangle}{\langle\alpha(\vec{\zeta}),\alpha^{\mathrm{xtal}}\rangle}\right)^2, \tag{A1}$$

which should range from 0 for amorphous to 1 for ideally crystalline structures. Using similar methods, perhaps related to an atom's bond-angle distribution, a bond orientation $\theta(\vec{\zeta})$ could be likewise assigned. Finally, the continuous fields could be defined through the following coarse-graining procedure:

$$\eta(\vec{x})e^{i\theta(\vec{x})} = \frac{\sum_{\mathrm{atoms}(j)}\int_{\mathcal{V}}\chi(\vec{x}-\vec{\zeta}_j)\,\eta(\vec{\zeta}_j)e^{i\theta(\vec{\zeta}_j)}dV}{\sum_{\mathrm{atoms}(j)}\int_{\mathcal{V}}\chi(\vec{x}-\vec{\zeta}_j)dV}, \tag{A2}$$

where $\chi(\vec{x})$ is a convolution function (i.e., with compact support) such as $\exp(-\vec{x}\cdot\vec{x}/\ell^2)$ where ℓ is a coarse-graining length, typically on the order of a few bond lengths.

[1] R. Kobayashi, J. A. Warren, and W. C. Carter, Physica D **140**, 141 (2000).
[2] J. W. Cahn, J. Chem. Phys. **66**, 3667 (1977).
[3] R. Vanselow and R. F. Howe, *Chemistry and Physics of Solid Surfaces*, Vol. 7 (Springer-Verlag, Berlin, 1988).
[4] J. W. Cahn, J. Phys. (Paris) **43**, 199 (1982), proceedings of Conference on the Structure of Grain Boundaries, Caen, France.
[5] E. W. Hart, Scr. Metall. **2**, 179 (1968).
[6] R. Kikuchi and J. W. Cahn, Phys. Rev. B **21**, 1893 (1980).
[7] J. W. Cahn and J. E. Hilliard, J. Chem. Phys. **28**, 258 (1958).
[8] D. Chatain and P. Wynblatt, Surf. Sci. **345**, 85 (1996).
[9] M. R. Moldover and J. W. Cahn, Science **207**, 1073 (1980).
[10] J. G. Dash, Contemp. Phys. **30**, 89 (1989).
[11] J. W. M. Frenken, P. M. J. Maree, and J. F. van der Veen, Phys. Rev. B **34**, 7506 (1986).
[12] J. W. M. Frenken and J. F. van der Veen, Phys. Rev. Lett. **54**, 134 (1985).
[13] D. Chatain and P. Wynblatt, in *Dynamics of Crystal Surfaces and Interfaces*, edited by P. M. Duxbury and T. J. Pence (Plenum Press, New York, 1997), pp. 53–58.
[14] B. Pluis, A. W. D. van der Gon, J. F. van der Veen, and A. J. Riemersma, Surf. Sci. **239**, 268 (1990).
[15] J. Lapujoulade, B. Salanon, F. Fabre, and B. Loisel, in *Kinetics of Ordering and Growth at Surfaces*, edited by M. G. Lagally (Plenum Press, New York, 1990), pp. 355–368.
[16] R. Lipowsky, U. Breuer, K. C. Prince, and H. P. Bonzel, Phys. Rev. Lett. **62**, 913 (1989).
[17] B. Pluis, D. Frenkel, and A. J. Riemersma, Surf. Sci. **239**, 282 (1990).
[18] J. F. van der Veen, in *Phase Transitions in Surface Films*, edited by H. Taub, G. Torzo, H. J. Lauter, and S. C. Fain Jr. (Plenum Press, New York, 1991), Vol. 2, pp. 289–305.
[19] J. F. van der Veen, B. Pluis, and A. W. D. van der Gon, in *Kinetics of Ordering and Growth at Surfaces*, edited by M. G. Lagally (Plenum Press, New York, 1990), pp. 343–354.
[20] D. W. Demianczuk and K. T. Aust, Acta Metall. **23**, 1149 (1975).
[21] H. Gleiter, Z. Metallkd. **61**, 282 (1970).
[22] E. L. Maksimova, L. S. Shvindlerman, and B. B. Straumal, Acta Metall. **36**, 1573 (1988).
[23] T. Watanabe, S. I. Kimura, and S. Karashima, Philos. Mag. A **49**, 845 (1984).
[24] K. Lücke and H.-P. Stüwe, Acta Metall. **19**, 1687 (1971).
[25] D. A. Molodov, U. Czubayko, G. Gottstein, and L. S. Shvindlerman, Acta Mater. **46**, 1573 (1998).
[26] T. Hsieh and R. Balluffi, Acta Metall. **37**, 1637 (1989).
[27] M. E. Glicksman and C. L. Vold, Surf. Sci. **31**, 50 (1972).
[28] G. Besold and O. G. Mouritsen, Phys. Rev. B **50**, 6573 (1994).
[29] G. Ciccotti, M. Guillope, and V. Pontikis, Phys. Rev. B **27**, 5576 (1983).
[30] G. A. Evangelakis, M. Hou, C. Maunier, and V. Pontikis, J. Phys. (Paris), Colloq. **51**, 127 (1990).
[31] P. Keblinski, S. R. Phillpot, D. Wolf, and H. Gleiter, Philos. Mag. Lett. **76**, 143 (1997).
[32] M. Meyer and C. Waldberger, Mater. Sci. Forum **126–128**, 229

(1993).
[33] T. Nguyen, P. S. Ho, T. Kwok, C. Nitta, and S. Yip, Phys. Rev. B **46**, 6050 (1992).
[34] S. R. Phillpot, J. F. Lutsko, D. Wolf, and S. Yip, Phys. Rev. B **40**, 2831 (1989).
[35] P. Deymier, A. Taiwo, and G. M. Kalonji, Acta Metall. **35**, 2719 (1987).
[36] T. Nguyen, P. S. Ho, T. Kwok, C. Nitta, and S. Yip, Phys. Rev. Lett. **57**, 1919 (1986).
[37] J. F. Lutsko, D. Wolf, S. R. Phillpot, and S. Yip, Phys. Rev. B **40**, 2841 (1989).
[38] S. J. Plimpton and E. D. Wolf, Phys. Rev. B **41**, 2712 (1990).
[39] V. Pontikis, J. Phys. (Paris) **49**, 327 (1988).
[40] L.-Q. Chen and G. Kalonji, Philos. Mag. A **66**, 11 (1992).
[41] S. M. Foiles, M. I. Baskes, and M. S. Daw, Mater. Res. Soc. Symp. Proc. **122**, 343 (1988).
[42] M. Guillope, J. Phys. (Paris) **47**, 1347 (1986).
[43] R. Najafabadi, D. J. Srolovitz, and R. Lesar, J. Mater. Res. **6**, 999 (1991).
[44] D. N. Seidman, Annu. Rev. Mater. Sci. **32**, 235 (2002).
[45] P. Keblinski, D. Wolf, S. R. Phillpot, and H. Gleiter, Philos. Mag. A **79**, 2735 (1999).
[46] B. Schönfelder, G. Gottstein, and L. S. Shvindlerman, Acta Mater. **53**, 1597 (2005).
[47] B. Schönfelder, P. Keblinski, D. Wolf, and S. R. Phillpot, Mater. Sci. Forum **294–96**, 9 (1999).
[48] R. Kobayashi, J. A. Warren, and W. C. Carter, Physica D **119**, 415 (1998).
[49] J. Warren, R. Kobayashi, A. Lobkovsky, and W. Carter, Acta Mater. **51**, 6035 (2003).
[50] A. Lobkovsky and J. Warren, Physica D **164**, 202 (2002).
[51] C. M. Bishop, M. Tang, R. M. Cannon, and W. C. Carter (unpublished).
[52] R. M. Cannon and L. Esposito, Z. Metallkd. **90**, 1002 (1999).
[53] Y.-M. Chiang, L. A. Silverman, R. H. French, and R. M. Cannon, J. Am. Ceram. Soc. **77**, 1143 (1994).
[54] H.-J. Kleebe, M. K. Cinibulk, R. M. Cannon, and M. Rühle, J. Am. Ceram. Soc. **76**, 1969 (1993).
[55] E. I. Rabkin, L. S. Shvindlerman, W. Gust, and B. B. Straumal, Mater. Sci. Forum **126–128**, 305 (1993).
[56] C. J. Simpson and K. T. Aust, Surf. Sci. **31**, 479 (1972).
[57] B. B. Straumal and W. Gust, Mater. Sci. Forum **207–209**, 59 (1996).
[58] B. B. Straumal, P. Zieba, and W. Gust, Int. J. Inorg. Mater. **3**, 1113 (2001).
[59] A. E. Lobkovsky and J. A. Warren, Phys. Rev. E **63**, 051605 (2001).
[60] R. Kobayashi and Y. Giga, J. Stat. Phys. **95**, 1187 (1999).
[61] I. Gelfand and S. Fomin, *Calculus of Variations* (Prentice-Hall, Inc., Englewood Cliffs, NJ, 1963).
[62] J. Q. Broughton and G. H. Gilmer, Phys. Rev. Lett. **56**, 2692 (1986).
[63] H. B. Aaron and G. F. Bolling, Surf. Sci. **31**, 27 (1972).
[64] R. Balluffi, Metall. Trans. A **13A**, 2069 (1982).
[65] N. A. Gjostein and F. N. Rhines, Acta Metall. **7**, 319 (1959).
[66] D. Wolf and K. L. Merkle, in *Materials Interfaces*, edited by D. Wolf and S. Yip (Chapman and Hall, London, 1992), pp. 87–150.
[67] D. Wolf, Scr. Metall. **23**, 1713 (1989).
[68] L.-Q. Chen and G. Kalonji, Philos. Mag. A **60**, 525 (1989).
[69] C. Counterman, L.-Q. Chen, and G. Kalonji, J. Phys. Colloq. **49**, 139 (1988).
[70] P. Keblinski, S. R. Phillpot, D. Wolf, and H. Gleiter, J. Am. Ceram. Soc. **80**, 717 (1997).
[71] S. W. Chan, J. S. Liu, and R. W. Balluffi, Scr. Metall. **19**, 1251 (1985).
[72] R. Balluffi and R. Maurer, Scr. Metall. **22**, 709 (1988).
[73] U. Erb and H. Gleiter, Scr. Metall. **13**, 61 (1979).
[74] U. Dahmen and K. H. Westmacott, in *Interface: Structure and Properties* (Trans Tech Publications, Switzerland, 1993), pp. 133–367.
[75] T. Hsieh and R. Balluffi, Acta Metall. **37**, 2133 (1989).
[76] R. H. French, J. Am. Ceram. Soc. **83**, 2117 (2000).
[77] K. van Benthem, G. Tan, L. K. DeNoyer, R. H. French, and M. Rühle, Phys. Rev. Lett. **93**, 227201 (2004).
[78] A. W. Denier van der Gon, J. M. Gay, J. W. M. Frenken, and J. F. van der Veen, Surf. Sci. **241**, 335 (1991).
[79] J. W. Herman and H. E. Elsayed-Ali, Phys. Rev. B **49**, 4886 (1994).
[80] X. Zeng and H. E. Elsayed-Ali, Phys. Rev. B **64**, 085410 (2001).
[81] I. Tanaka, H.-J. Kleebe, M. K. Cinibulk, J. Bruley, D. R. Clarke, and M. Rühle, J. Am. Ceram. Soc. **77**, 911 (1994).
[82] C.-M. Wang, X. Pan, M. J. Hoffmann, R. M. Cannon, and M. Rühle, J. Am. Ceram. Soc. **79**, 788 (1996).
[83] H. Wang and Y.-M. Chiang, J. Am. Ceram. Soc. **81**, 89 (1998).
[84] H. Gu, X. Pan, R. M. Cannon, and M. Rühle, J. Am. Ceram. Soc. **81**, 3125 (1998).
[85] H. Gu, R. M. Cannon, and M. Rühle, J. Mater. Res. **13**, 376 (1998).
[86] H. Gu, R. Cannon, H. Seifert, M. Hoffmann, and I. Tanaka, J. Am. Ceram. Soc. **85**, 25 (2002).
[87] H. Gu, R. Cannon, I. Tanaka, and M. Rühle (unpublished).
[88] R. Zallen, *The Physics of Amorphous Solids* (Wiley-Interscience, New York, 1998).
[89] C. M. Bishop and W. C. Carter, Comput. Mater. Sci. **25**, 378 (2002).
[90] A. P. Sutton, in *Materials Research Society Proceedings* (Materials Research Society, Warrendale, PA, 1988), Vol. 122, pp. 81–96.
[91] In this paper, "interfaces" refers to both free surfaces—which separate a solid phase from a liquid or vapor phase—and grain boundaries—which separate two identical crystalline phases with differing orientations. We introduce "complexion" as the two-dimensional analog to a bulk phase: parts of an interface that differ with respect to any equilibrium feature are examples of different complexions of the same interface
[92] While crystal symmetry is not treated here, the set of possible orientations should be reduced by considerations of symmetry.